Structural Engineering and Mechanics, *Vol. 55, No. 3 (2015) 473-494*
DOI: http://dx.doi.org/10.12989/sem.2015.55.3.473

Application of graded harmonic FE in the analysis of 2D-FGM axisymmetric structures

Ali I. Karakas and Ayse T. Daloglu*

Department of Civil Engineering, Karadeniz Technical University, 61080 Trabzon, Turkey

(Received November 29, 2014, Revised April 21, 2015, Accepted April 27, 2015)

Abstract. A graded harmonic finite element formulation based on three-dimensional elasticity theory is developed for the structural analysis of 2D functionally graded axisymmetric structures. The mechanical properties of the axisymmetric solid structures composed of two different metals and ceramics are assumed to vary in radial and axial directions according to power law variations as a function of the volume fractions of the constituents. The material properties of the graded element are calculated at the integration points. Effects of material distribution profile on the static deformation, natural frequency and dynamic response analyses of particular axisymmetric solid structures are investigated by changing the power law exponents. It is observed that the displacements, stresses and natural frequencies are severely affected by the variation of axial and radial power law exponents. Good accuracy is obtained with fewer elements in the present study since Fourier series expansion eliminates the need of finite element mesh in circumferential direction and continuous material property distribution within the elements improves accuracy without refining the mesh size in axial and radial directions.

Keywords: computational mechanics; finite element method (FEM); functionally graded; numerical methods; parametric analysis

1. Introduction

Functionally graded materials (FGMs) are the combination of two or more different materials. The volume fractions of these materials vary uniformly along certain directions. Therefore, FGMs have a non-uniform microstructure and a continuously variable macrostructure. They were first introduced by a Japanese research group to address the need of aggressive environment of thermal shock (Koizumi 1993). FGMs possess a number of advantages that make them attractive in potential applications, including a potential reduction of in-plane and transverse stress through the thickness, an improved residual stress distribution, enhanced thermal properties, higher fracture toughness and reduced stress intensity factors (Birman and Byrd 2007).

Several studies are available in the literature on FGM structures. Praveen and Reddy (1998) investigated the static and dynamic thermoelastic responses of plates made of functionally graded materials. Loy *et al.* (1999), Pradhan *et al.* (2000), Asgari and Akhlaghi (2011) obtained natural frequencies of FGM cylinders under various conditions. Han *et al.* (2001) analyzed transient

*Corresponding author, Professor, E-mail: aysed@ktu.edu.tr

http://www.techno-press.org/?journal=sem&subpage=8 ISSN: 1225-4568 (Print), 1598-6217 (Online)

waves in FGM cylinders. Shakeri *et al.* (2006) analyzed radial wave propagation in FGM cylinders with infinite length by FEM. They considered the FGM cylinder as a multilayer cylinderwith constant material properties for each layer. Hosseini *et al.* (2007) analyzed the same problem considering variable material properties in the layers. Foroutan and Moradi-Dastjerdi (2011) carried out dynamic analysis of FGM cylinders that were subjected to an impact load by a mesh free method.

Several numerical models have been used to investigate FGMs. For instance, Paulino and Jin (2000) used integral equations, Aboudi *et al.* (1999), Pindera and Dunn (1997) used higher order theory and Goldberg and Hopkins (1995), Sutradhar *et al.* (2002) used boundary element method. Also, conventional finite elements are used by Li *et al*. (2001), Marur and Tippur (2000). Moreover, graded finite elements are developed for the analysis of FGM structures. The graded finite elements incorporates the material property gradient at the size scale of the element, while conventional elements produce a step-wise constant approximation to a continuous material property field. Graded elements are implemented by means of direct sampling properties at the Gauss points of the element. Santare and Lambros (2000), Kim and Paulino (2002), Buttlar *et al*. (2006), Santare *et al.* (2003), Taghvaeipour *et al.* (2012) are the researchers developed graded elements.

In this study a graded harmonic finite element formulation based on three-dimensional elasticity theory for the structural analysis of 2D functionally graded axisymmetric structures is presented. The first phase of the study is focused on determining volume fraction and material distribution in 2D-Functionally graded materials. In Section 3, a ring of quadrilateral cross section with nine nodes is considered as graded harmonic model which is based on a displacement field described by Fourier series for axisymmetric structures. Obtaining of FEM model of the problem using Hamilton's principle is mentioned in Section 4. Formulations of the element stiffness matrix, mass matrix and element force vector are expressed in Section 5, respectively. Finally, a number of various functionally graded axisymmetric problems are solved to demonstrate static, free and forced vibration responses.

2. Volume fraction and material distribution in 2D-FGM

Two-dimensional FGMs are usually made by continuous gradation of three or four distinct material phases where one or two are ceramics and the others are metal alloy phases.

The volume fractions of the constituents vary in a predetermined composition profile. Now

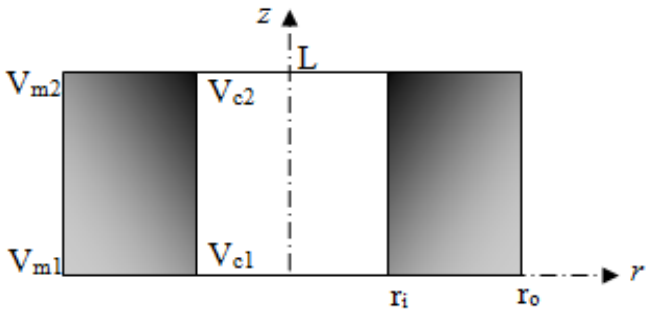

Fig. 1 Axisymmetric cylinder with two-dimensional material distribution

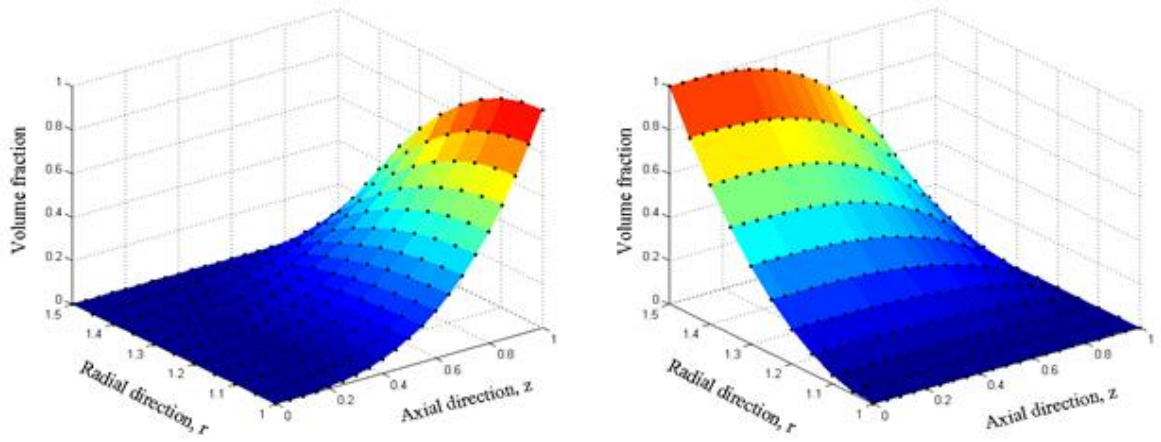

(a) (b)

Fig. 2 Volume fraction distribution of (a) *c*2 and (b) *m*1 for n_r=2 and n_z=3

consider the volume fractions of 2D-FGM at any arbitrary point in the 2D-FG axisymmetric cylinder with inner radius r_i, outer radius r_o, and finite length L as shown in Fig. 1. In the present cylinder the inner surface is made of two distinct ceramics and the outer surface of two metals. While *c*1, *c*2 denote the first and second ceramic, *m*1 and *m*2 denote for the first and second metal, respectively.

The volume fraction of the first ceramic material is changed from 100% at the lower surface to zero at the upper surface by a power law function. Also this volume fraction is changed continuously from inner to outer surface. Volume fractions of the other materials change similarly in two directions. The volume fraction distribution function of each material can be expressed as

$$V_{c1} = \left[1-\left(\frac{r-r_i}{r_o-r_i}\right)^{n_r}\right]\left[1-\left(\frac{z}{L}\right)^{n_z}\right] \tag{1a}$$

$$V_{c2} = \left[1-\left(\frac{r-r_i}{r_o-r_i}\right)^{n_r}\right]\left(\frac{z}{L}\right)^{n_z} \tag{1b}$$

$$V_{m1} = \left(\frac{r-r_i}{r_o-r_i}\right)^{n_r}\left[1-\left(\frac{z}{L}\right)^{n_z}\right] \tag{1c}$$

$$V_{m2} = \left(\frac{r-r_i}{r_o-r_i}\right)^{n_r}\left(\frac{z}{L}\right)^{n_z} \tag{1d}$$

where power law exponents n_r and n_z are non-zero parameters that represent the basic constituent distributions in radial-*r* and axial-*z* directions (Asgari *et al*. 2009). Volume fraction distributions of

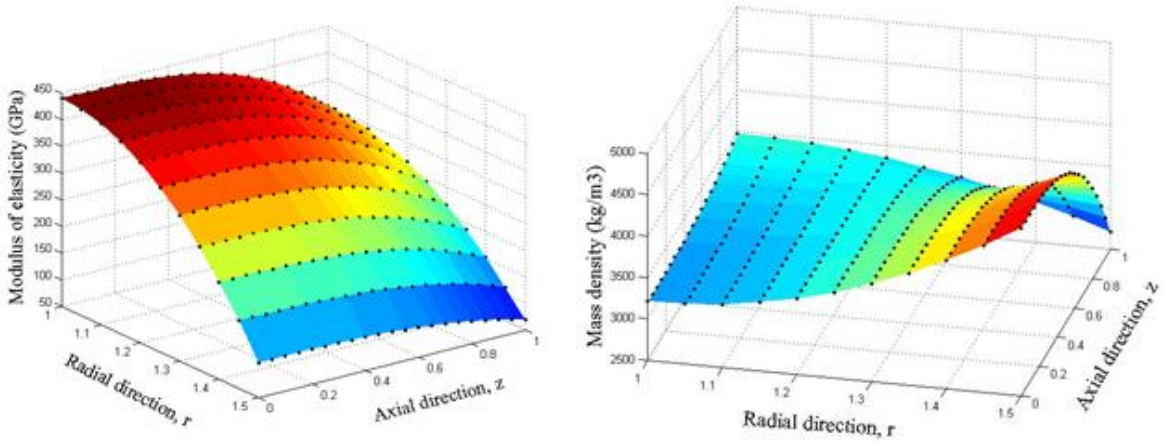

(a) (b)

Fig. 3 Variation of (a) modulus of elasticity and (b) mass density through the cylinder for n_r=2 and n_z=3

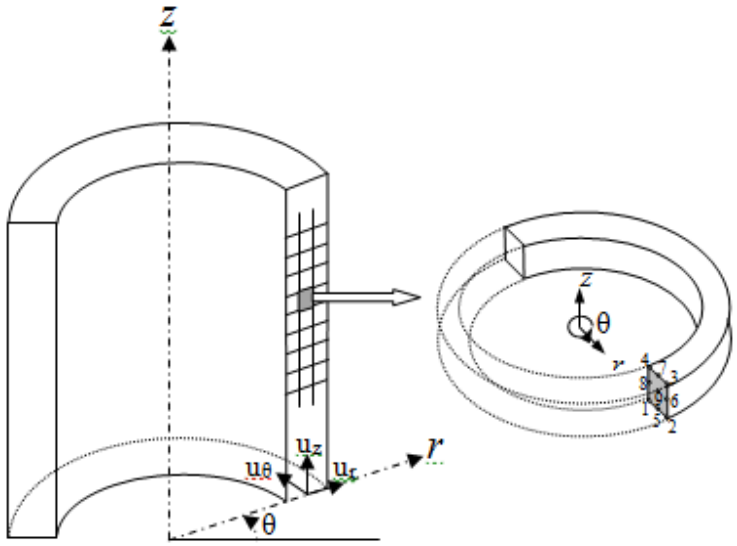

Fig. 4 Displacement components and an axisymmetric finite element

two basic materials for the typical values of n_r=2 and n_z=3 are shown in Fig. 2 as an example by taking r_i=1 m, r_o=1.5 m, and L=1 m.

Material properties at any point can be obtained by using the linear rule of mixtures, in which a material property, P, at an arbitrary point (r, z) in the 2D-FGM cylinder is determined by linear combination of volume fractions and material properties of the basic materials as

$$P(r,z) = P_{c1}V_{c1} + P_{c2}V_{c2} + P_{m1}V_{m1} + P_{m2}V_{m2} \quad (2)$$

The variation of a material property such as Young's modulus through the cylinder is shown in Fig. 3 for the typical values of n_r=2 and n_z=3.

3. Graded harmonic model

For axisymmetric structures, a ring of quadrilateral cross section with nine nodes is considered (see Fig. 4). The center of all nodal circles lies on the *z*-axis, which is the axis of revolution.

The present model is based on a displacement field described by Fourier series as

$$\{u\}=\begin{Bmatrix}u_r(r,\theta,z)\\ u_\theta(r,\theta,z)\\ u_z(r,\theta,z)\end{Bmatrix}=\begin{Bmatrix}\sum_{m=0}^{Nh}\bar{u}_{rm}\cos m\theta+\sum_{m=0}^{Nh}\bar{\bar{u}}_{rm}\sin m\theta\\ \sum_{m=0}^{Nh}\bar{u}_{\theta m}\sin m\theta-\sum_{m=0}^{Nh}\bar{\bar{u}}_{\theta m}\cos m\theta\\ \sum_{m=0}^{Nh}\bar{u}_{zm}\cos m\theta+\sum_{m=0}^{Nh}\bar{\bar{u}}_{zm}\sin m\theta\end{Bmatrix} \tag{3}$$

where m is the circumferential harmonic number, Nh is the total number of harmonics and symbols u_r, u_θ and u_z indicate the radial, circumferential and axial displacement components, respectively, see Fig. 4 (Cook *et al.* 1989). In Eq. (3) all barred quantities are amplitudes approximated using the finite element method, which are functions of r, z but not of θ. This leads to a harmonic finite element in the (r, z) plane. Single barred amplitudes represent symmetric displacement components while double barred amplitudes represent anti-symmetric displacement terms. The negative sign in the circumferential displacement is important to achieve the same stiffness matrix for $m\neq 0$. The amplitudes of the displacement components for a finite element can be interpolated as

$$\{u\}=\sum_{m=0}^{Nh}\left(\left[\overline{g_{\theta m}}\right]_u[N]\{\bar{d}_m\}+\left[\overline{\overline{g_{\theta m}}}\right]_u[N]\{\bar{\bar{d}}_m\}\right) \tag{4}$$

where $[N]$ is the matrix of assumed shape functions, $\{\bar{d}_m\}$ and $\{\bar{\bar{d}}_m\}$ are nodal displacement amplitudes vectors and $\left[\overline{g_{\theta m}}\right]_u$ and $\left[\overline{\overline{g_{\theta m}}}\right]_u$ are the matrices of harmonic functions for displacements. Details are given in Appendix. The shape functions for the displacements within a graded harmonic finite element and the strain-displacement relations are the same as standard conventional elements. The strain displacement relations in cylindrical coordinates is given by

$$\{\varepsilon\}=\begin{Bmatrix}\varepsilon_r\\ \varepsilon_\theta\\ \varepsilon_z\\ \gamma_{rz}\\ \gamma_{r\theta}\\ \gamma_{\theta z}\end{Bmatrix}=\begin{Bmatrix}\dfrac{\partial u_r}{\partial r}\\ \dfrac{1}{r}(u_r+\dfrac{\partial u_\theta}{\partial\theta})\\ \dfrac{\partial u_z}{\partial z}\\ \dfrac{\partial u_z}{\partial r}+\dfrac{\partial u_r}{\partial z}\\ \dfrac{1}{r}\dfrac{\partial u_r}{\partial\theta}+\dfrac{\partial u_\theta}{\partial r}-\dfrac{u_\theta}{r}\\ \dfrac{\partial u_\theta}{\partial z}+\dfrac{1}{r}\dfrac{\partial u_z}{\partial\theta}\end{Bmatrix}=\sum_{m=0}^{Nh}\left(\left[\overline{g_{\theta m}}\right]_\varepsilon[B_m]\{\bar{d}_m\}+\left[\overline{\overline{g_{\theta m}}}\right]_\varepsilon[B_m]\{\bar{\bar{d}}_m\}\right) \tag{5}$$

where $[B_m]$ is the matrix which relate the nodal displacement amplitudes with corresponding strains for the m^{th} harmonic and $\left[\overline{g_{\theta m}}\right]_{\varepsilon}$ and $\left[\overline{\overline{g_{\theta m}}}\right]_{\varepsilon}$ are the matrices of harmonic functions for strains (Cook *et al.* 1989).

The constitutive equation for functionally graded materials are written as

$$\{\sigma\} = [D(r,z)]\{\varepsilon\} \tag{6}$$

where $[D(r, z)]$ is the elasticity matrix as given in (Cook *et al.* 1989) for a three dimensional isotropic material. However, Young's modulus and Poisson's ratio are not constant material properties for each finite element. They are specified at each Gaussian integration point according to Eq. (2). In other words, the elasticity matrix is assumed to be a function of spatial coordinates within the element to describe the actual material property gradient.

4. Equation of motion

The finite element model of the problem can be obtained directly from Hamilton's principle.

$$\int_{t_1}^{t_2} \delta(U - T - W)dt = 0 \tag{7}$$

where U and T are strain and kinetic energy respectively, and W is work done by surface tractions. These functions are expressed as

$$U = \frac{1}{2}\int_V \{\varepsilon\}^T \{\sigma\}\, dV \tag{8}$$

$$T = \frac{1}{2}\int_V \rho\{\dot{u}\}^T \{\dot{u}\}\, dV \tag{9}$$

$$W = \int_A \{u\}^T \{F_s\}\, dA \tag{10}$$

where A and V denote the area and volume of the domain under consideration and F_s is the surface traction vector. Surface tractions can be expresses in terms of Fourier harmonics as

$$\{F_s\} = \sum_{m=0}^{Nh}\left(\left[\overline{g_{\theta m}}\right]_u \left\{\bar{q}_{sm}\right\} + \left[\overline{\overline{g_{\theta m}}}\right]_u \left\{\bar{\bar{q}}_{sm}\right\}\right) \tag{11}$$

where $\left\{\bar{q}_{sm}\right\}$ and $\left\{\bar{\bar{q}}_{sm}\right\}$ are the symmetric and anti-symmetric surface load amplitude vectors for harmonic m, respectively. The Hamilton's principle is applied for each element by substituting Eqs. (8)-(11) and (4)-(6) into Eq. (7) and the following expression is obtained for harmonic m

$$\begin{bmatrix} \delta\left\{\bar{d}_m^{\,e}\right\}^T \\ \delta\left\{\bar{\bar{d}}_m^{\,e}\right\}^T \end{bmatrix} \left[\int_{V_e} [B_m]^T \begin{bmatrix} \left[\overline{g_{\theta m}}\right]_{\varepsilon}^T [D]\left[\overline{g_{\theta m}}\right]_{\varepsilon} & \left[\overline{g_{\theta m}}\right]_{\varepsilon}^T [D]\left[\overline{\overline{g_{\theta m}}}\right]_{\varepsilon} \\ \left[\overline{\overline{g_{\theta m}}}\right]_{\varepsilon}^T [D]\left[\overline{g_{\theta m}}\right]_{\varepsilon} & \left[\overline{\overline{g_{\theta m}}}\right]_{\varepsilon}^T [D]\left[\overline{\overline{g_{\theta m}}}\right]_{\varepsilon} \end{bmatrix} [B_m] dV \right] \begin{bmatrix} \left\{\bar{d}_m^{\,e}\right\} \\ \left\{\bar{\bar{d}}_m^{\,e}\right\} \end{bmatrix}$$

$$
\begin{aligned}
&+\begin{bmatrix} \delta\{\bar{d}_m^{\,e}\}^T \\ \delta\{\bar{\bar{d}}_m^{\,e}\}^T \end{bmatrix}\left[\int_{V_e}\rho[N]^T\begin{bmatrix} [\overline{g_{\theta m}}]_u^T[\overline{g_{\theta m}}]_u & [\overline{g_{\theta m}}]_u^T[\overline{\overline{g_{\theta m}}}]_u \\ [\overline{\overline{g_{\theta m}}}]_u^T[\overline{g_{\theta m}}]_u & [\overline{\overline{g_{\theta m}}}]_u^T[\overline{\overline{g_{\theta m}}}]_u \end{bmatrix}[N]dV\right]\begin{bmatrix} \{\ddot{\bar{d}}_m^{\,e}\} \\ \{\ddot{\bar{\bar{d}}}_m^{\,e}\} \end{bmatrix} \\
&=\begin{bmatrix} \delta\{\bar{d}_m^{\,e}\}^T \\ \delta\{\bar{\bar{d}}_m^{\,e}\}^T \end{bmatrix}\left[\int_{A_e}[N]^T\begin{bmatrix} [\overline{g_{\theta m}}]_u^T[\overline{g_{\theta m}}]_u & [\overline{g_{\theta m}}]_u^T[\overline{\overline{g_{\theta m}}}]_u \\ [\overline{\overline{g_{\theta m}}}]_u^T[\overline{g_{\theta m}}]_u & [\overline{\overline{g_{\theta m}}}]_u^T[\overline{\overline{g_{\theta m}}}]_u \end{bmatrix}\begin{bmatrix} \{\bar{q}_{sm}\} \\ \{\bar{\bar{q}}_{sm}\} \end{bmatrix}dA\right]
\end{aligned}
\tag{12}
$$

$\delta\{\bar{d}_m^{\,e}\}$ and $\delta\{\bar{\bar{d}}_m^{\,e}\}$ can be omitted from Eq. (12) since they are some arbitrary variational displacement amplitudes of the nodal points of an element. Then this equation of motion can be written for harmonic *m* as

$$
\begin{bmatrix} [\bar{k}_m]\{\bar{d}_m^e\}+[\bar{m}_m]\{\ddot{\bar{d}}_m^e\} \\ [\bar{\bar{k}}_m]\{\bar{\bar{d}}_m^e\}+[\bar{\bar{m}}_m]\{\ddot{\bar{\bar{d}}}_m^e\} \end{bmatrix}=\begin{bmatrix} \{\bar{f}_{sm}\} \\ \{\bar{\bar{f}}_{sm}\} \end{bmatrix}
\tag{13}
$$

where $[\bar{k}_m]$, $[\bar{m}_m]$ and $\{\bar{f}_{sm}\}$ are the element stiffness matrix, mass matrix and force vector for harmonic *m* and single barred terms in Fourier series expansion, respectively.

5. Graded finite element equations

5.1 Formulation of the element stiffness matrix

Two stiffness matrices $[\bar{k}_m]$ and $[\bar{\bar{k}}_m]$are calculated for both single and double barred terms in Fourier series expansion from the strain energy in Eq. (12) as

$$
[\bar{k}_m]=\iint_{A_e}[B_m]^T\left(\int_0^{2\pi}[\overline{g_{\theta m}}]_\varepsilon^T[D(r,z)][\overline{g_{\theta m}}]_\varepsilon d\theta\right)[B_m]rdrdz
\tag{14}
$$

$$
[\bar{\bar{k}}_m]=\iint_{A_e}[B_m]^T\left(\int_0^{2\pi}[\overline{\overline{g_{\theta m}}}]_\varepsilon^T[D(r,z)][\overline{\overline{g_{\theta m}}}]_\varepsilon d\theta\right)[B_m]rdrdz
\tag{15}
$$

where A_e is the cross-sectional area of the element on the *r*-*z* plane. It can be observed that each term in the products of $[\overline{g_{\theta m}}]_\varepsilon^T[D(r,z)][\overline{g_{\theta m}}]_\varepsilon$ and $[\overline{\overline{g_{\theta m}}}]_\varepsilon^T[D(r,z)][\overline{\overline{g_{\theta m}}}]_\varepsilon$ will be a function of (*E*, *v*) multiplied by either $\cos^2 m\theta$ or $\sin^2 m\theta$. Thus, integration over the circumferential direction θ can be carried out explicitly using orthogonality of trigonometric functions as

$$
\int_0^{2\pi}[\overline{g_{\theta m}}]_\varepsilon^T[D(r,z)][\overline{g_{\theta m}}]_\varepsilon d\theta=\begin{cases}\pi[D(r,z)] & \text{for m>0}\\ [\bar{D}_0(r,z)] & \text{for m=0}\end{cases}
\tag{16}
$$

$$\int_0^{2\pi} \left[\overline{\overline{g_{\theta m}}}\right]_\varepsilon^T [D(r,z)] \left[\overline{\overline{g_{\theta m}}}\right]_\varepsilon d\theta = \begin{cases} \pi[D(r,z)] & \text{for m>0} \\ [\bar{\bar{D}}_0(r,z)] & \text{for m=0} \end{cases} \tag{17}$$

where $[\bar{D}_0(r,z)]$ and $[\bar{\bar{D}}_0(r,z)]$ are given in Appendix. It should also be mentioned that, due to the choice of negative sign in the second expression in Eq. (3), the stiffness matrix for double barred terms is identical to that of single barred terms, that is $[\bar{k}_m]=[\bar{\bar{k}}_m]=[k_m]$ for $m>0$. Additionally, $[\bar{k}_0]$ and $[\bar{\bar{k}}_0]$ can be used for particular cases of plane axisymmetric and plane axi-antisymmetric cases for $m=0$, respectively. So, the stiffness matrices are obtained from the following expressions using Gauss integration procedure as

$$\left[\bar{k}_0\right] = \sum_{k=1}^{3}\sum_{l=1}^{3} w_k w_l \left[B_m(\xi_k,\eta_l)\right]^T \left[\bar{D}_0(\xi_k,\eta_l)\right] \left[B_m(\xi_k,\eta_l)\right] r(\xi_k,\eta_l) J(\xi_k,\eta_l) \tag{18}$$

$$\left[\bar{\bar{k}}_0\right] = \sum_{k=1}^{3}\sum_{l=1}^{3} w_k w_l \left[B_m(\xi_k,\eta_l)\right]^T \left[\bar{\bar{D}}_0(\xi_k,\eta_l)\right] \left[B_m(\xi_k,\eta_l)\right] r(\xi_k,\eta_l) J(\xi_k,\eta_l) \tag{19}$$

$$\left[k_m\right] = \sum_{k=1}^{3}\sum_{l=1}^{3} w_k w_l \left[B_m(\xi_k,\eta_l)\right]^T \left[D(\xi_k,\eta_l)\right] \left[B_m(\xi_k,\eta_l)\right] r(\xi_k,\eta_l) J(\xi_k,\eta_l) \quad \text{for m >0} \tag{20}$$

where ξ_k and η_l are the Gauss points, w_k and w_l are the corresponding integration weights and $[D(\xi_k, \eta_l)]$ is the value of elasticity matrix at the respective Gauss points.

5.2 Formulation of the element mass matrix

The consistent mass matrix of an element is calculated from the derivation of the kinetic energy in Eq. (12). The mass matrices for single and double barred terms of an element for the Fourier term m can be taken out as

$$\left[\bar{m}_m\right] = \iint_{A_e} \rho(r,z) [N]^T \left(\int_0^{2\pi} \left(\left[\overline{g_{\theta m}}\right]_u^T \left[\overline{g_{\theta m}}\right]_u \right) d\theta \right) [N] r dr dz \tag{21}$$

$$\left[\bar{\bar{m}}_m\right] = \iint_{A_e} \rho(r,z) [N]^T \left(\int_0^{2\pi} \left(\left[\overline{\overline{g_{\theta m}}}\right]_u^T \left[\overline{\overline{g_{\theta m}}}\right]_u \right) d\theta \right) [N] r dr dz \tag{22}$$

The integrals can be carried out explicitly with respect to circumferential direction as in the case of the stiffness matrix equations. The integrals will result in a factor π for harmonics greater than zero for both single and double barred terms. Therefore, $[\bar{m}_m]=[\bar{\bar{m}}_m]=[m_m]$ is valid for $m>0$. Likewise stiffness equations, Gauss numerical integration procedure is used and the following element mass matrices are obtained for harmonics as

$$\left[\bar{m}_0\right] = 2\pi \sum_{k=1}^{3}\sum_{l=1}^{3} w_k w_l \rho(\xi_k,\eta_l) N^T(\xi_k,\eta_l) \begin{bmatrix} 1 & 0 & 0 \\ 0 & 0 & 0 \\ 0 & 0 & 1 \end{bmatrix} N(\xi_k,\eta_l) r(\xi_k,\eta_l) J(\xi_k,\eta_l) \tag{23}$$

$$\left[\overline{\overline{m}}_0\right] = 2\pi \sum_{k=1}^{3}\sum_{l=1}^{3} w_k w_l \rho(\xi_k,\eta_l) N^T(\xi_k,\eta_l) \begin{bmatrix} 0 & 0 & 0 \\ 0 & 1 & 0 \\ 0 & 0 & 0 \end{bmatrix} N(\xi_k,\eta_l) r(\xi_k,\eta_l) J(\xi_k,\eta_l) \tag{24}$$

$$\left[m_m\right] = \pi \sum_{k=1}^{3}\sum_{l=1}^{3} w_k w_l \rho(\xi_k,\eta_l) N^T(\xi_k,\eta_l) N(\xi_k,\eta_l) r(\xi_k,\eta_l) J(\xi_k,\eta_l) \quad \text{for (m>0)} \tag{25}$$

where $\rho(\xi_k, \eta_l)$ represents the mass density evaluated at Gauss points *k*, *l*.

5.3 Formulation of the element force vector

The consistent surface traction vector is calculated from the derivation of the external work done by surface load in Eq. (12). The consistent surface traction vectors for the Fourier term *m* due to surface force can be expressed as

$$\left\{\overline{f}_{sm}\right\} = \int \left[N\right]^T \left(\int_0^{2\pi} \left(\left[\overline{g_{\theta m}}\right]_u^T \left[\overline{g_{\theta m}}\right]_u \right) d\theta \right) \left\{\overline{q}_{sm}\right\} ds \tag{26}$$

$$\left\{\overline{\overline{f}}_{sm}\right\} = \int \left[N\right]^T \left(\int_0^{2\pi} \left(\left[\overline{\overline{g_{\theta m}}}\right]_u^T \left[\overline{\overline{g_{\theta m}}}\right]_u \right) d\theta \right) \left\{\overline{\overline{q}}_{sm}\right\} ds \tag{27}$$

where, $ds = \sqrt{dr^2 + dz^2}$. Taking integrals with respect to the circumferential direction θ and using one-dimensional Gauss integration the following expressions are obtained

$$\begin{aligned} \{\overline{f}_{s0}\} &= 2\pi \sum_{k=1}^{3} w_k \left[N(\xi_k)\right]^T \begin{bmatrix} 1 & 0 & 0 \\ 0 & 0 & 0 \\ 0 & 0 & 1 \end{bmatrix} \{q_{s0}\} r(\xi_k) J_\Gamma(\xi_k) \\ \{\overline{\overline{f}}_{s0}\} &= 2\pi \sum_{k=1}^{3} w_k \left[N(\xi_k)\right]^T \begin{bmatrix} 0 & 0 & 0 \\ 0 & 1 & 0 \\ 0 & 0 & 0 \end{bmatrix} \{q_{s0}\} r(\xi_k) J_\Gamma(\xi_k) \end{aligned} \quad \text{for m=0} \tag{28}$$

$$\begin{aligned} \{\overline{f}_{sm}\} &= \pi \sum_{k=1}^{3} w_k \left[N(\xi_k)\right]^T \{\overline{q}_{sm}\} r(\xi_k) J_\Gamma(\xi_k) \\ \{\overline{\overline{f}}_{sm}\} &= \pi \sum_{k=1}^{3} w_k \left[N(\xi_k)\right]^T \{\overline{\overline{q}}_{sm}\} r(\xi_k) J_\Gamma(\xi_k) \end{aligned} \quad \text{for m>0} \tag{29}$$

where J_Γ is the associated arc length Jacobian.

6. Verification of the graded harmonic element

Table 1 Comparison of deformations of a FGM hollow cylinder subjected to various static loadings (L=2 m, r_i=0.2 m, r_o=0.4 m E_{c1}=E_{c2}=110 GPa, E_{m1}=E_{m2}=400 GPa, ν_{c1}=ν_{c2}=0.34, ν_{c1}=ν_{c2}=0.28, n_r=3, n_z=0)

	Maximum elongation(m)		
	(2)[a]	(5)	(10)
Taghvaeipour *et al.* (2012)	2.620e-7	2.760e-7	2.870e-7
Present	2.759e-7	2.876e-7	2.914e-7
	Maximum deflection(m)		
	(10)	(12)	(15)
Taghvaeipour *et al.* (2012)	-7.420e-6	-7.520e-6	-7.610e-6
Present	-7.590e-6	-7.598e-6	-7.606e-6
	Maximum rotation(rad)		
	(2)	(5)	(10)
Taghvaeipour *et al.* (2012)	14.52e-7	14.60e-7	14.35e-7
Present	15.26e-6	15.75e-6	15.87e-6
	Isotropic metal	Isotropic ceramic	
Exact	8.25e-6	31.43e-6	

[a]The bracketed numbers indicate the number of element

Table 2 Comparison of natural frequencies (Hz) for clamped-clamped functionally graded hollow cylinders (L=2 m, r_i=0.2 m, E_{c1}=E_{c2}=110 GPa, E_{m1}=E_{m2}=400 GPa, ν_{c1}=ν_{c2}=0.34, ν_{c1}=ν_{c2}=0.28, ρ_{c1}=ρ_{c2}=8960 kg/m^3, ρ_{m1}=ρ_{m2}=19300 kg/m^3, n_r=3, n_z=0, h=r_o-r_i)

h/r_i	First bending mode			Torsion mode		
	Present (6-117)	Taghvaeipour *et al.* (2012)		Present (3-63)	Taghvaeipour *et al.* (2012)	
		Superele.	Brick		Superele.	Brick
		(30[a]-744[b])	(3000-3410)		(30-744)	(3000-3410)
0.2	357	369	357	624	639	622
0.4	381	391	379	631	646	629
0.6	401	413	400	636	652	634
0.8	420	434	418	641	656	639
1	437	453	436	644	660	642
1.2	453	470	452	647	662	645
1.4	467	486	462	649	665	647
1.6	479	500	477	651	667	649
1.8	490	513	487	652	668	650
2	500	525	497	654	670	652

A functionally graded hollow cylinder subjected to various static loads is considered to verify the graded harmonic element. One end of the cylinder is fixed and the free end is subjected to an axial tension of F=10 kN, a lateral load of P=10 kN, and an axial torque of T=24 kN.m. The maximum elongation, deflection and rotation of the cylinder are given in Table 1. The results obtained in the study are compared with the ones obtained by Taghvaeipour *et al.* (2012) and good agreements are obtained except for maximum rotations. Large differences in rotations are proved to be due to the typing errors in the values presented by Taghvaeipour *et al.* (2012). It should be noted that the results for functionally graded material have to be in between the results for

isotropic constituent materials. However, the rotations provided in (Taghvaeipour *et al.* 2012) do not fall in between the exact rotations obtained from mechanics of materials using small deformation theory for isotropic cylinders made of constituent metal and ceramic materials as given in Table 1. Also, it can be seen from Table 1 that the graded harmonic element has higher convergence rates.

Additionally, the natural frequencies for the first bending mode and torsion mode of clamped-clamped functionally graded cylinders with varying wall thickness to inner radius ratios are compared with the results obtained from the graphs provided by Taghvaeipour *et al.* (2012). The natural frequencies are presented in Table 2. It is seen that the present harmonic model requires very few elements to provide good accuracy. It should be emphasized that the number of graded harmonic elements can be increased due to nonlinear shape of bending mode for better results.

7. Numerical examples

After the verification of the proposed graded harmonic element, a number of various functionally graded axisymmetric problems are analyzed to investigate static, free and forced vibration responses. Mechanical properties of the constituent materials of two distinct ceramics and two distinct metals are presented in Table 3 to be used for the following examples.

7.1 Non-axisymmetrically loaded circular plate

The first problem is a simply-supported (SS) circular plate bent by a non-axisymmetric uniformly distributed load as shown in Fig. 5. The radius of the plate is r_o=10 m and thickness is

Table 3 Mechanical properties of constituent materials

Constituents	Material	E (GPa)	ρ (kg/m^3)	v
$m1$	Ti6Al4V	115	2715	0.342
$m2$	Al 1100	69	4515	0.330
$c1$	SiC	440	3210	0.140
$c2$	Al_2O_3	150	3470	0.210

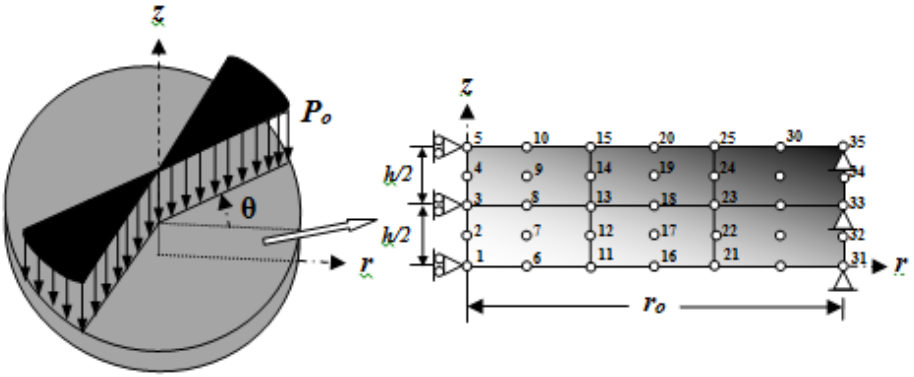

Fig. 5 Loading and sample discretization of the circular plate problem

Table 4 Fourier coefficients for non-axisymmetric loading

$\bar{q}_{zsm}$	$\bar{\bar{q}}_{zsm}$
8.3333 (m=0)	15.9154 (m=2)
−13.7832 (m=4)	−10.6103 (m=6)
6.8916 (m=8)	3.1830 (m=10)
−3.4458 (m=16)	2.2736 (m=14)
2.7566 (m=20)	−3.5367 (m=18)
−1.9690 (m=28)	1.4468 (m=22)
1.7229 (m=32)	1.2242 (m=26)
−1.3783 (m=40)	−2.1220 (m=30)
1.2530 (m=44)	0.9362 (m=34)

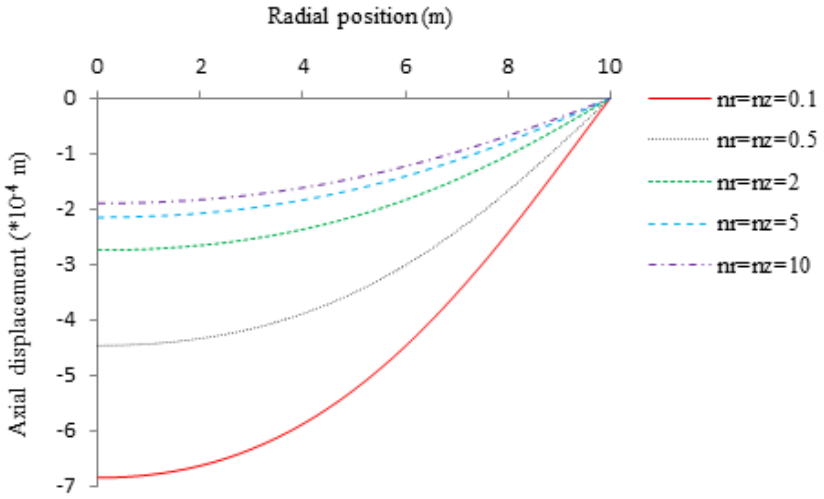

Fig. 6 Axial displacements along the bottom plate surface at θ=45°

h=1 m. The distributed load of magnitude P_o=50 kN/m^2 acts downward at the second and eighth slice of circular plate which is divided into thirty degree slices. The axial loading is approximated using Fourier coefficients for corresponding single and double barred harmonics. The axial load components for corresponding harmonics are given in Table 4. Sample finite element discretization and support conditions are pictured in Fig. 5.

Fig. 6 and 7 depict the axial deflections and radial stresses along the bottom surface of the circular plate for a number of various power law exponents equal in radial and axial directions. It is seen from Fig. 6 that the axial displacement increases with decreasing power law exponents in both directions and the maximum displacement is obtained for n_r=n_z=0.1. However, the maximum radial stress is obtained for n_r=n_z=0.5. Therefore, it can be concluded that the nonhomogeneous distribution of material using different can affect the maximum values. The desired properties can be obtained by optimizing the power law components. For example, the nonhomogeneous material distribution can be organized in accordance with the loading position in the structure to control the response to the loading. Fig. 8 shows the radial stress distribution contour on the bottom plate surface for a particular power law exponent, n_r=n_z=2, in both the directions.

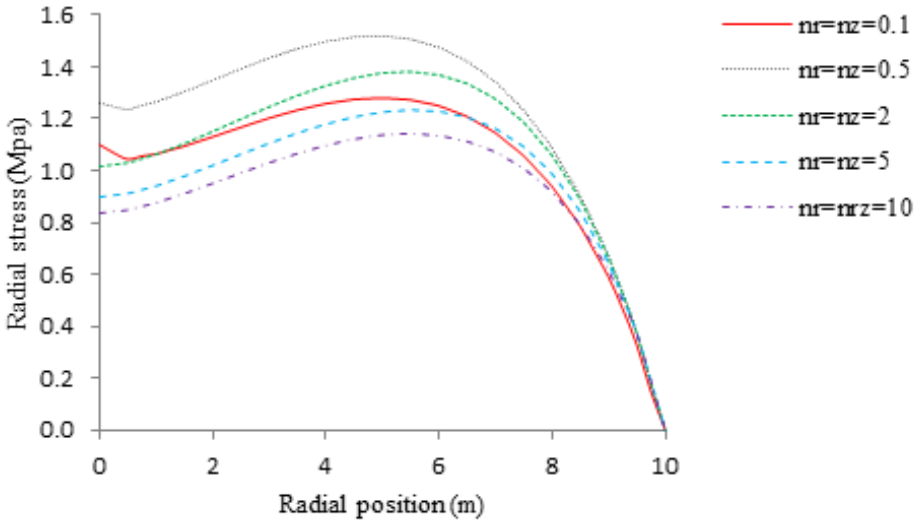

Fig. 7 Radial stresses along the bottom plate surface at θ=45^o

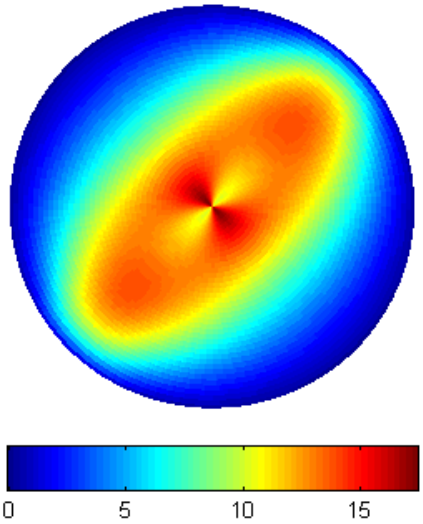

Fig. 8 Radial stress ($x10^2$ kPa) distribution on the bottom plate surface (n_r=n_z=2)

7.2 Rotating thin disc

The second problem is a hollow, thin circular disc of thickness h=0.01 m, inner radius r_i=0.04 m, and outer radius r_o=0.1 m, which spins about the z axis with constant angular frequency of ω=1000 rad/s. Sample finite element discretization and support conditions are shown in Fig. 9. The motion is accommodated by constraining nodes at the bottom surface to be on rollers as shown in Fig. 9. All other nodes are kept free. The only load is a centrifugal body force acting along radial direction (Karakaş 2012).

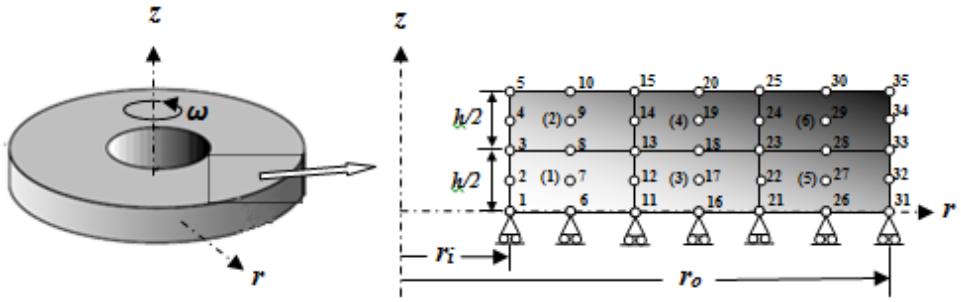

Fig. 9 Sample discretization and support conditions of the rotating disc

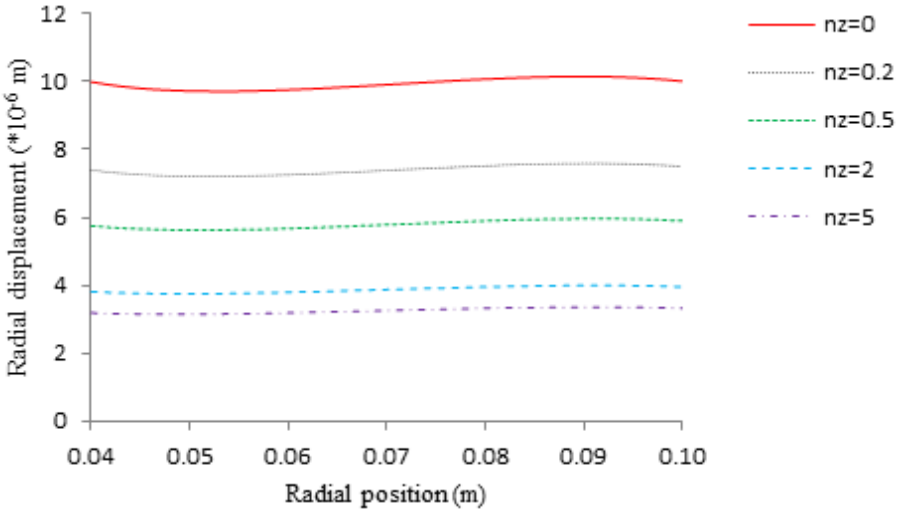

Fig. 10 Radial displacements along the middle disc surface for n_r=2

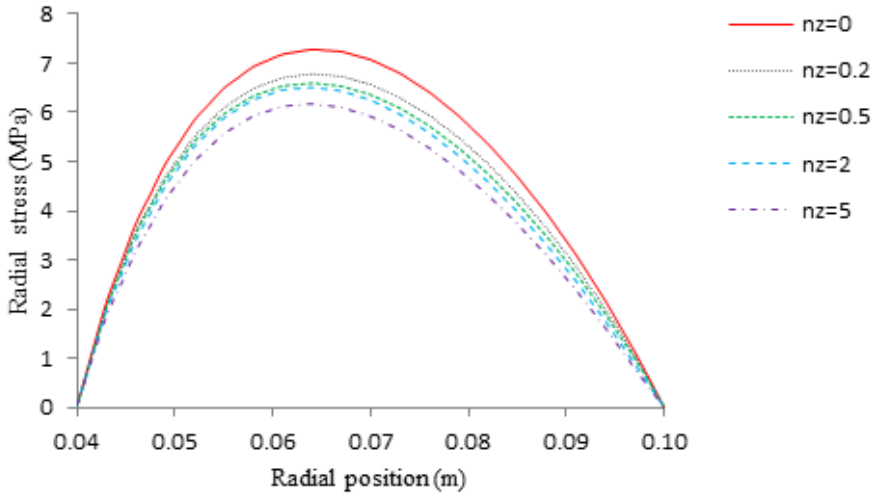

Fig. 11 Radial stresses along the middle disc surface for n_r=2

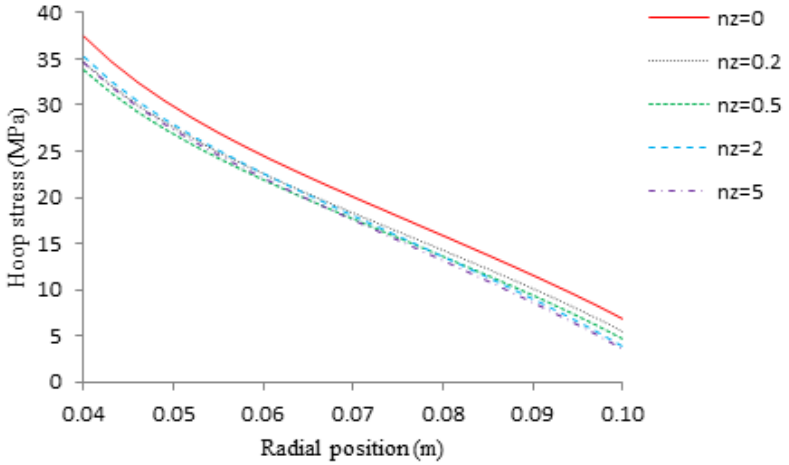

Fig. 12 Hoop stresses along the middle disc surface for n_r=2

Figs. 10, 11 and 12 show the radial displacement, radial and hoop stresses along the wall thickness of the middle surface of the rotating disc for a number of various power law exponents in axial direction when radial power law exponent is n_r=2. As can be seen radial displacement, radial and hoop stresses decrease with increasing axial power law exponent n_z. Increasing the volume fraction of m1 and c1 material in the nonhomogeneous material by increasing axial power law exponent n_z decreases the displacement and stresses considerably as shown in the figures. Therefore, it can be stated that the maximum magnitude of responses can be controlled by using different volume fraction configurations in functionally graded nonhomogeneous material.

7.3 Free vibration of finite length hollow cylinders

The third problem is the natural frequency analysis of a simply-simply supported thick hollow functionally graded cylinder of wall thickness h=0.2 m, inner radius r_i=0.2 m, and length L=1 m. Additionally, the fundamental natural frequencies are obtained for various ratios of wall thickness to inner radius.

Fig. 13 shows that the natural frequencies of the thick-walled cylinder increase with increasing circumferential harmonic number m and axial power law exponent n_z. Fig. 14(a) shows the variations in the fundamental natural frequencies with wall thickness to inner radius ratio h/r_i and axial power law exponent n_z. The fundamental natural frequencies increase with increasing volume fractions of m1 and c1 materials in nonhomogeneous material gradation of the cylinders and h/r_i ratio as shown in Fig. 14(a). Therefore, it can be concluded that by altering nonhomogeneous material distribution the free vibration characteristics of structures can be controlled as desired.

The circumferential harmonic number m at which the fundamental frequency occurs is observed to decrease until a particular h/r_i ratio as seen in Fig. 14(b). This means that when h/r_i is beyond a certain value, which is h/r_i=0.3 in this case, the fundamental natural frequencies would occur at the circumferential harmonic number m=1. The value of the axial power law exponent n_z does not affect the circumferential harmonic number at which the fundamental natural frequency occurs. In other words, for each h/r_i ratio corresponding to all axial power law exponents the fundamental natural frequencies occur at the same circumferential harmonic number m.

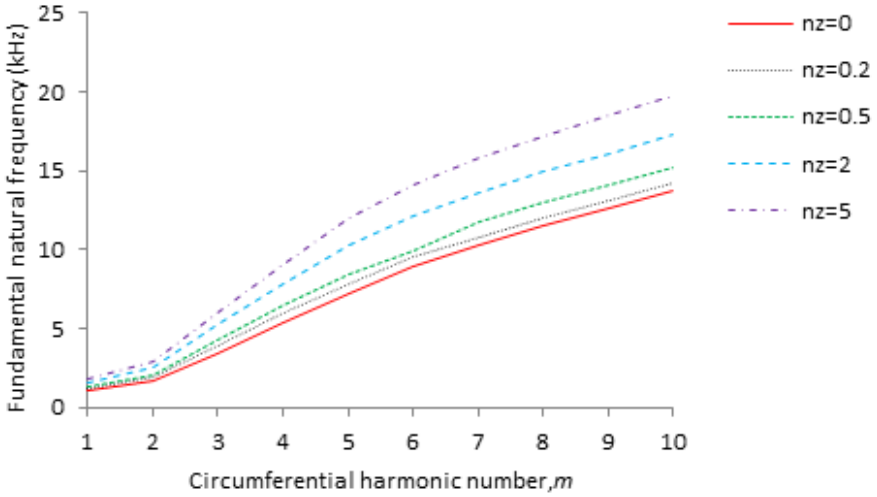

Fig. 13 Variation of natural frequency with circumferential harmonic number for various axial power law exponents (n_r=2, h/r_i=1)

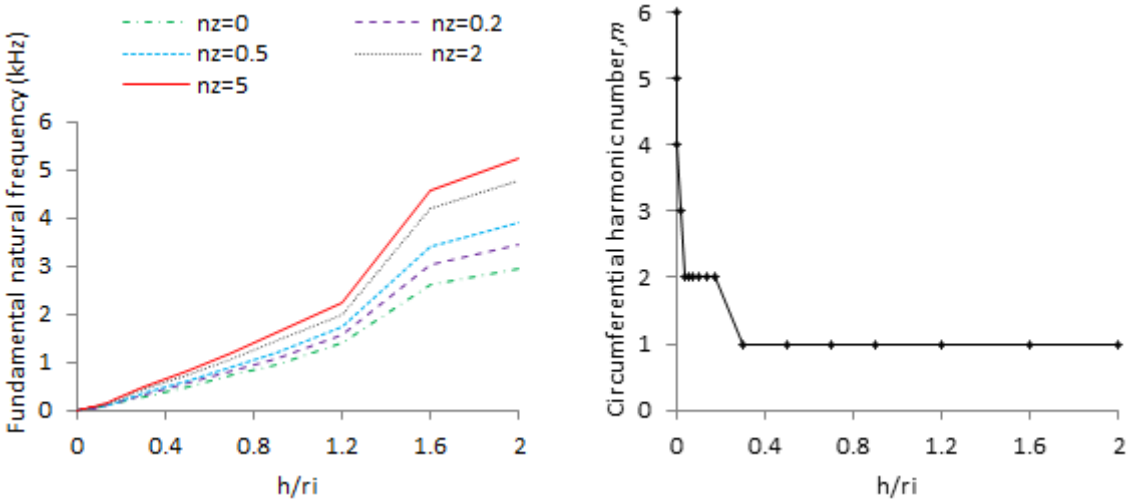

(a) (b)

Fig. 14 Variation of (a) fundamental natural frequency (kHz) and (b) circumferential harmonic number m with h/r_i for various axial power law exponents (n_r=2)

7.4 Dynamic analysis of a hollow infinite cylinder

A FGM cylinder of inner radius r_i=0.25 m and outer radius r_o=0.5 m subjected to an internal pressure expressed by

$$P(t)=P_o\sin\left(\frac{\pi t}{0.0002}\right) \quad \text{for} \quad t \le 0.0002\text{s}$$
$$P(t)=0 \quad \text{for} \quad t > 0.0002\text{s}. \tag{30}$$

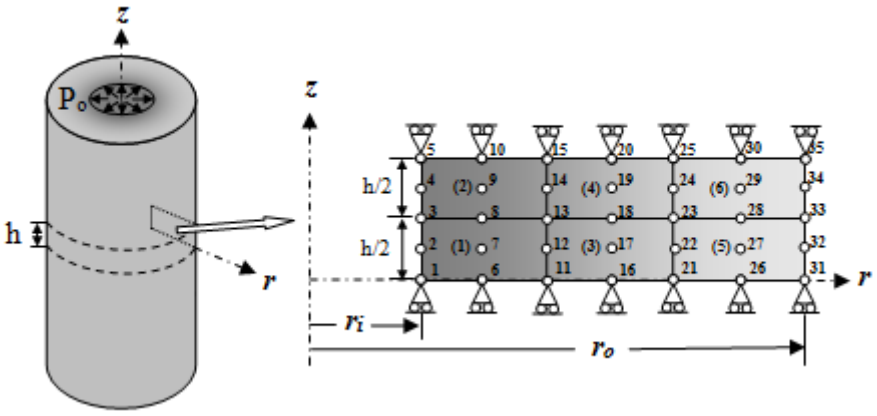

Fig. 15 Pressurized cylinder: sample discretization and support conditions

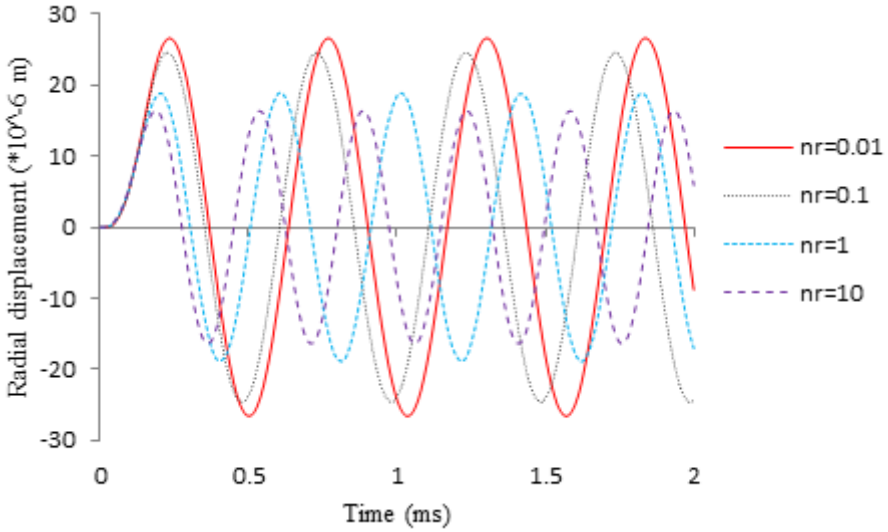

Fig. 16 Radial displacement of the midpoint (r=0.375 m) of the FGM infinite cylinder (n_z=0)

where P_o=4 GPa/s and t is time in second is considered as the last example. The cylinder extends indefinitely along the axial direction and is in a plane strain state along that direction. Nodes move in the radial direction only as shown in Fig. 15. A slice of thickness h=0.1 m is extracted and discretized for the analysis (Fig. 15). The material variation in radial direction is only considered since the cylinder is infinitely long in axial direction. The differential equations of motion are solved using Newmark-beta method.

Fig. 16 shows the radial displacement of the midpoint of the cylinder (r=0.375 m). This figure indicates that for larger amounts of n_r, the amplitude and period of vibration decrease. Figs. 17 and 18 depict time variations of radial and hoop or circumferential stresses at the same point. These figures reveal that the stress wave speed gets larger as n_r gets smaller. Also the maximum radial and hoop stresses occur for n_r=0.1 and n_r=10, respectively. It is evident from these figures that

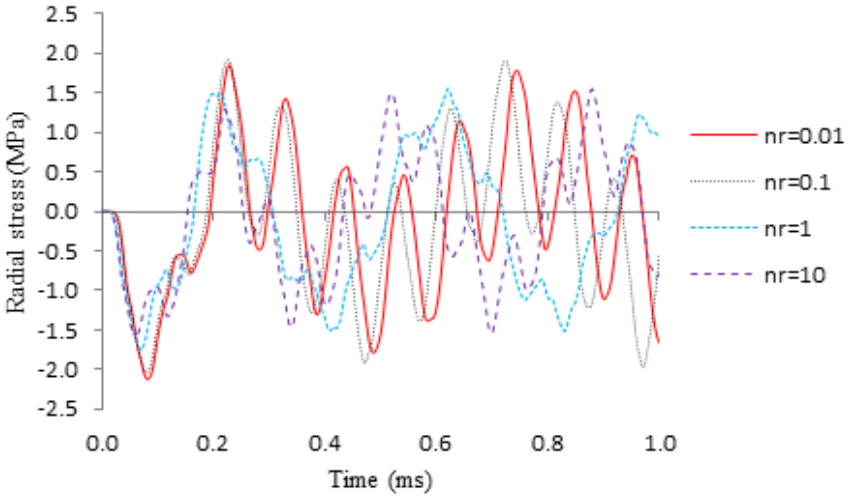

Fig. 17 Radial stress of the midpoint (r=0.375 m) of the FGM infinite cylinder (n_z=0)

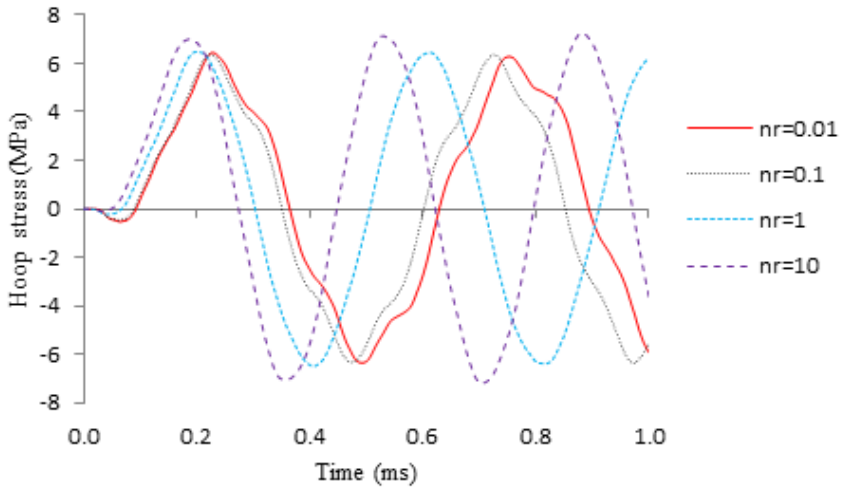

Fig. 18 Hoop stress of the midpoint (r=0.375 m) of the FGM infinite cylinder (n_z=0)

both of amplitude and time delay of the response are strongly affected by the power law exponent n_r. Therefore, it can be stated that the magnitude and occurrence time of maximum dynamic responses can be controlled by the modification of nonhomogeneous material distribution of the structure to be considered.

8. Conclusions

This paper presents the development and applications of the graded harmonic finite element for one or two dimensional functionally graded (FG) axisymmetric structures. The theoretical

formulation based on three-dimensional elasticity theory of a nine-node graded harmonic ring element is presented. Material properties of the graded elements are calculated at each integration point using a power law distribution model. For the verification of the graded element static deformation and frequency analyses are conducted. The results show good agreement with those obtained by other elements that presented in the literature. The static, free and dynamic analyses of FG axisymmetric structures are performed later. At first, static deformation and stress analyses of a non-axisymmetrically loaded FG circular plate and a rotating FG disc are conducted. Then, the graded element is used for frequency analysis of various hollow FG cylinders. At last, a FG cylinder with infinite length under impact dynamic loading is studied. The dynamic responses are developed and the variations of different parameters with power law exponents are obtained. It is observed that static and dynamic displacements, stresses and natural frequencies are severely affected by the variation of axial and radial power law exponents. Therefore, using various gradation of nonhomogeneous functionally graded material the magnitude of critical displacements and stresses can be controlled as well as the locations and timings of maximums. In this way the opportunity of controlling the failure of structures can be obtained. Also, the free vibration characteristics of the structures can be altered as desired by changing material distribution properties. Such favorable properties of FGM materials and the responses of structures can be obtained by using the developed graded harmonic ring finite elements as shown in the numerical examples. Finally, it can be concluded that the graded harmonic model requires very few elements to provide good accuracy since Fourier series expansion eliminates the need to mesh in circumferential direction and continuous material property distribution within the elements improves accuracy without refining the mesh size in axial and radial directions.

Acknowledgements

The first author has been supported by TUBITAK (Turkish Scientific and Technological Research Council) with a scholarship which is gratefully acknowledged.

References

Aboudi, J., Pindera, M.J. and Arnold, S.M. (1999), "Higher- order theory for functionally graded materials", *Compos. Part B*, **30**, 777-832.

Asgari, M. and Akhlaghi, M. (2011), "Natural frequency analysis of 2D-FGM thick hollow cylinder based on three-dimensional elasticity equations", *Eur. J. Mech. A Solid.*, **30**, 72-81.

Asgari, M., Akhlaghi, M. and Hosseini, S.M. (2009), "Dynamic analysis of two-dimensional functionally graded thick hollow cylinder with finite length under impact loading", *Acta Mech*., **208**, 163-180.

Birman, V. and Byrd, L.W. (2007), "Modeling and analysis of functionally graded materials and structures", *Appl. Mech. Rev.*, **60,** 195-215.

Buttlar, W.G., Paulino, H.H. and Song, S.H. (2006), "Application of graded finite elements for asphalt pavements", *J. Eng. Mech*., **132**, 240-249.

Cook, R.D., Malkus, D.S. and Plesha, M.E. (1989), *Concepts and Applications of Finite Element Analysis*, 3rd Edition, Wiley&Sons.

Foroutan, M. and Moradi-Dastjerdi, R. (2011), "Dynamic analysis of functionally graded material cylinders under an impact load by a mesh-free method", *Acta Mech*., **219**, 281-290.

Goldberg, R.K. and Hopkins, D.A. (1995), "Thermal analysis of a functionally graded material subject to a

thermal gradient using the boundary element method", *Compos. Meth. Appl. Mech. Eng.*, **5**(7), 793-806.
Han, X., Liu, G.R., Xi, Z.C. and Lam, K.Y. (2001), "Transient waves in a functionally graded cylinder", *Int. J. Solid. Struct*., **38**, 3021-3037.
Hosseini, S.M., Akhlaghi, M. and Shakeri, M. (2007), "Dynamic response and radial wave propagation velocity in thick hollow cylinder made of functionally graded materials", *Int. J. Comput. Aid. Eng. Softw.*, **24**, 288-303.
Karakaş, A.İ. (2012), "Static and dynamic analyses of axisymmetric structures using Harmonic Solid Ring Finite Element Modeling", Master dissertation, Karadeniz Technical University, Turkey.
Kim, J.H. and Paulino, G.H. (2002), "Isoparametric graded finite elements for nonhomogeneous isotropic and orthotropic materials", *J. Appl. Mech*., **69**, 502-514.
Koizumi, M. (1993), "The concept of FGM.", *Ceram. Tran. Funct. Gradient Mater*., **51**, 28-32.
Li, Y., Ramesh, K.T. and Chin, E.S.C. (2001), "Dynamic characterization of layered and graded structures under impulsive loading", *Int. J. Solid. Struct*., **38**, 6045-6061.
Loy, C.T., Lam, K.Y. and Reddy, J.N. (1999), "Vibration of functionally graded cylindrical shells", *Int. J. Mech. Sci.*, **41**, 309-324.
Marur, P.R. and Tippur, H.V. (2000), "Numerical analysis of crack-tip fields in functionally graded materials with a crack normal to the elastic gradient*", Int. J. Solid. Struct*., **37**, 5353-5370.
Paulino, G.H. and Jin, Z.H. (2000), "Viscoelastic functionally graded materials subjected to antiplane shear fracture", *ASME J. Appl. Mech*., **68**(1), 284-293.
Pindera, M.J. and Dunn, P. (1997), "Evaluation of the higher-order theory for functionally graded materials via the finite element method", *Compos. Part B*, **28**, 109-119.
Praveen, G.N. and Reddy, J.N. (1998), "Nonlinear transient thermoelastic analysis of functionally graded ceramic-metal plates", *Int. J. Solid. Struct*., **35**, 4457-4476.
Pradhan, S.C., Loy, C.T., Lam, K.Y. and Reddy, J.N. (2000), "Vibration characteristics functionally graded cylindrical shells under various boundary conditions", *Appl. Acoust.*, **61**, 111-129.
Shakeri, M., Akhlaghi, M. and Hosseini, S.M. (2006), "Vibration and radial wave propagation velocity in functionally graded thick hollow cylinder", *Compos. Struct*., **76**, 174-181.
Santare, M.H. and Lambros, J. (2000), "Use of graded finite elements to model the behavior of nonhomogeneous materials", *J. Appl. Mech*., **67**, 819-822.
Santare, M.H., Thamburaj, P. and Gazonas, G.A. (2003), "The use of graded finite elements in the study of elastic wave propagation in continuously nonhomogeneous materials" *Int. J. Solid. Struct.*, **40**, 5621-5634.
Sutradhar, S., Paulino, G.H. and Gray, L.J. (2002), "Transient heat conduction in homogenous and non-homogeneous materials by the laplace transform Galerkin boundary element method", *Eng. Anal. Bound. Elem*., **26**, 119-132.
Taghvaeipour, A., Bonakdar, M. and Ahmadian, M.T. (2012), "Application of a new cylindrical element formulation in finite element structural analysis of FGM hollow cylinders", *Finite Elem. Anal. Des*., **50**, 1-7.

CC

Appendix

The shape function matrix is

$$[N]=\begin{bmatrix}[N]_1 & [N]_2 & ..... & [N]_9\end{bmatrix} \text{ where } [N]_i=\begin{bmatrix} N_i & 0 & 0 \\ 0 & N_i & 0 \\ 0 & 0 & N_i \end{bmatrix} \tag{1}$$

and its components are

$$\begin{aligned} N_i &= \frac{1}{4}\xi\eta[(\xi+\xi_i)(\eta+\eta_i) \quad \text{for i=1,2,3,4} \\ N_i &= \frac{1}{2}\eta(1-\xi_i\xi^2)(\eta+\eta_i) \qquad \text{for i=5,7} \\ N_i &= \frac{1}{2}\xi(\xi+\xi_i)(1-\eta_i\eta^2) \qquad \text{for i=6,8} \\ N_9 &= (1-\xi^2)(1-\eta^2) \end{aligned} \tag{2}$$

where $\xi_i=(-1,1,1,-1,1,1,1,-1)$ and $\eta_i=(-1,-1,1,1,-1,1,1,1)$

The matrices of harmonic functions for displacements and strains are

$$\left[\overline{g_{\theta m}}\right]_u=\begin{bmatrix} \mathrm{c} & . & . \\ . & \mathrm{s} & . \\ . & . & \mathrm{c} \end{bmatrix} \text{ and } \left[\overline{\overline{g_{\theta m}}}\right]_u=\begin{bmatrix} \mathrm{s} & . & . \\ . & -\mathrm{c} & . \\ . & . & \mathrm{s} \end{bmatrix} \tag{3}$$

$$\left[\overline{g_{\theta m}}\right]_\varepsilon=\begin{bmatrix} c & . & . & . & . & . \\ . & c & . & . & . & . \\ . & . & c & . & . & . \\ . & . & . & c & . & . \\ . & . & . & . & s & . \\ . & . & . & . & . & s \end{bmatrix} \text{ and } \left[\overline{\overline{g_{\theta m}}}\right]_\varepsilon=\begin{bmatrix} s & . & . & . & . & . \\ . & s & . & . & . & . \\ . & . & s & . & . & . \\ . & . & . & s & . & . \\ . & . & . & . & -c & . \\ . & . & . & . & . & -c \end{bmatrix} \tag{4}$$

where c=cos $m\theta$, s=sin $m\theta$ and dots are zeros .

The strain-nodal displacement amplitude matrix

$$[B_m]=\begin{bmatrix} B_{1m} & B_{2m} & ... & B_{9m} \end{bmatrix} \tag{5}$$

Sub-matrix for the i^{th} node and harmonic m is

$$[B_{im}]=\begin{bmatrix} N_{i,r} & 0 & 0 \\ \dfrac{N_i}{r} & \dfrac{mN_i}{r} & 0 \\ 0 & 0 & N_{i,z} \\ N_{i,z} & 0 & N_{i,r} \\ -\dfrac{mN_i}{r} & (N_{i,r}-\dfrac{N_i}{r}) & 0 \\ 0 & N_{i,z} & -\dfrac{mN_i}{r} \end{bmatrix} \tag{6}$$

Elasticity matrices for harmonic m=0 (dots are zeros)

$$[\bar{D}_0(r,z)] = 2\pi \begin{bmatrix} 1 & \cdot & \cdot & \cdot & \cdot & \cdot \\ \cdot & 1 & \cdot & \cdot & \cdot & \cdot \\ \cdot & \cdot & 1 & \cdot & \cdot & \cdot \\ \cdot & \cdot & \cdot & 1 & \cdot & \cdot \\ \cdot & \cdot & \cdot & \cdot & \cdot & \cdot \\ \cdot & \cdot & \cdot & \cdot & \cdot & \cdot \end{bmatrix} [D(r,z)] \quad \text{and} \tag{7}$$

$$[\bar{\bar{D}}_0(r,z)] = 2\pi \begin{bmatrix} \cdot & \cdot & \cdot & \cdot & \cdot & \cdot \\ \cdot & \cdot & \cdot & \cdot & \cdot & \cdot \\ \cdot & \cdot & \cdot & \cdot & \cdot & \cdot \\ \cdot & \cdot & \cdot & \cdot & \cdot & \cdot \\ \cdot & \cdot & \cdot & \cdot & 1 & \cdot \\ \cdot & \cdot & \cdot & \cdot & \cdot & 1 \end{bmatrix} [D(r,z)] \tag{8}$$

$$\{\bar{q}_{sm}\} = \begin{Bmatrix} \bar{q}_{rsm} \\ \bar{q}_{\theta sm} \\ \bar{q}_{zsm} \end{Bmatrix} \quad \text{and} \quad \{\bar{\bar{q}}_{sm}\} = \begin{Bmatrix} \bar{\bar{q}}_{rsm} \\ \bar{\bar{q}}_{\theta sm} \\ \bar{\bar{q}}_{zsm} \end{Bmatrix} \tag{9}$$